Scientific Research

Research on the Application of Circumferential Prestressing Technology in Precast Concrete Wind Turbine Tower Structures

Kangle Chen, Di Yao and Sihang Wei *

ZRD New Energy Solutions Co., Ltd., Shanghai 201108, China.
* Correspondence: weisihang@zwindtowers.com

Abstract: The continuous increase in the single-unit capacity of wind turbines and the continuous increase in the hub height have led to new requirements for the structural performance of wind turbine towers. Precast prestressed concrete towers that are widely used in the field for large turbines and high towers are gradually replacing traditional steel towers on the market. However, research on structural joints, especially vertical joints where several precast concrete pieces are assembled into a ring segment, is limited. One way to improve the integrity of the structure and clarify the load path is to apply circumferential prestressing to the annular precast tower containing vertical structural joints. With the structural design example in a certain concrete wind tower project, this paper analyzes the effects of different magnitudes of circumferential prestressing on the structural performance under the service loads and the ultimate loads and proposes a method to determine the optimized design of the structure.

Keywords: concrete wind turbine tower; prestressing; precast; structural joints, finite element analysis

Citation: Chen, K.; Yao, D.; Wei, S. Research on the Application of Circumferential Prestressing Technology in Precast Concrete Wind Turbine Tower Structures. *Prestress Technology* **2024**, *3*, 20-33. https://doi.org/10.59238/j.pt.2024.03.003

Received: 07/09/2024
Accepted: 25/09/2024
Published: 30/09/2024

1 Introduction

In recent years, with the continuous increase in the rated power, rotor diameter and hub height of wind turbines, precast concrete wind turbine towers have been widely increasingly used due to better structural performance, lower cost, and ability to avoid structural resonance[1,2]. In the case of wind turbines with a hub height greater than 120 m, traditional steel towers are more and more difficult to perfectly match the requirements in design, construction, full-life cycle operation, maintenance, and cost. Where wind power has entered the era of bidding up the power market, precast concrete towers already possess the market environment and technical maturity for mass construction [3].

At present, the commonly used concrete wind tower design mostly adopts the precast, prestressed, schemes; that is, the concrete wind turbine tower is assembled on site from concrete ring segments of different sizes, and the diameter of the precast segments can gradually decrease from bottom to top. Each ring segment can be produced as a whole or in pieces and assembled on site. Vertical prestress is always applied from bottom to top, both ends anchored in tower foundation and the top concrete segment. The application of longitudinal prestress significantly increases the flexural capacity of a segmental precast wind tower; in addition, by increasing the cross-sectional bearing stress, it also increases the friction-shear capacity and tower structure integrity.

By splitting the full ring segment (as shown in Figure 1) into multiple precast concrete pieces (as shown in Figure 2), it makes considerable advantages in terms of the flexibility in transportation and the preparation of formworks. However, for the segments with vertical splits, the applied ultimate bending moment associated with large torsion and horizontal shear force, can also be a severe challenge to the integrity of its structure. To improve the structural behavior, most concrete towers require

 https://doi.org/10.59238/j.pt.2024.03.003

grouting at structural joints, which consumes a big volume of grout materials and increases the onsite assembly difficulties and duration. Moreover, grouting process is easily affected by temperature and weather conditions, the construction quality and time could be difficult to control. For the joints employing embedded steel parts and bolts, the bond slip between the embedded parts and the concrete as well as the local spalling of the concrete under cyclical loads will reduce the structural capacity, which leads to substantial tower deterioration. And thus, the above characters might create uneven stress concentrations, which is not beneficial to meet seismic requirements.

To address the issue associated with grouting connections with bolts, the practice of applying circumferential prestressing to an annular towering segment with multiple vertical joints can improve the integrity of the structure make the load-path more straight forward. In addition, it can help to make the structural layout more flexible, to reduce the construction duration, and help to reduce the construction cost. Another benefit is the circumferential prestressing steel strands do not necessarily require grouting, the quality and prestress loss are usually well predictable.

Figure 1 Full-ring precast segmental concrete wind turbine towers

Figure 2 Precast concrete segments with vertical joints

2 Case Study

Herein, a concrete wind turbine tower (built in 2023, China) with a hub height of 160 m (Figure 3 a)) is used as an example, the effect of circumferential prestressing is analyzed and discussed. This hybrid tower structure consists of a 132m concrete portion at the bottom and a 28 m steel portion at the top, where the steel tower connects the concrete base with the wind turbine nacelle. The concrete tower is divided into 44 ring segments along the height direction, each was designed with a height of 3m. Each segment of the tower is composed of three 120° tower pieces, and the vertical joints between the adjacent two ring segments are staggered. Epoxy grout was used on horizontal joints between ring segments and the vertical joints between concrete pieces. After the tower is erected, the longitudinal prestressed steel strands

running through the tower are tensioned to ensure the tower design capacity. Each bundle of prestressed steel strands has a total of 1 × 18 high-strength, low-relaxation ϕ^s15.2cables (nominal diameter of 15.2 mm) with a tensile strength of 1860 MPa, and the tension control stress is 70% of the material yield strength. The anchors, cable clamps, dampers and other ancillary facilities are shown in Figure 3d).

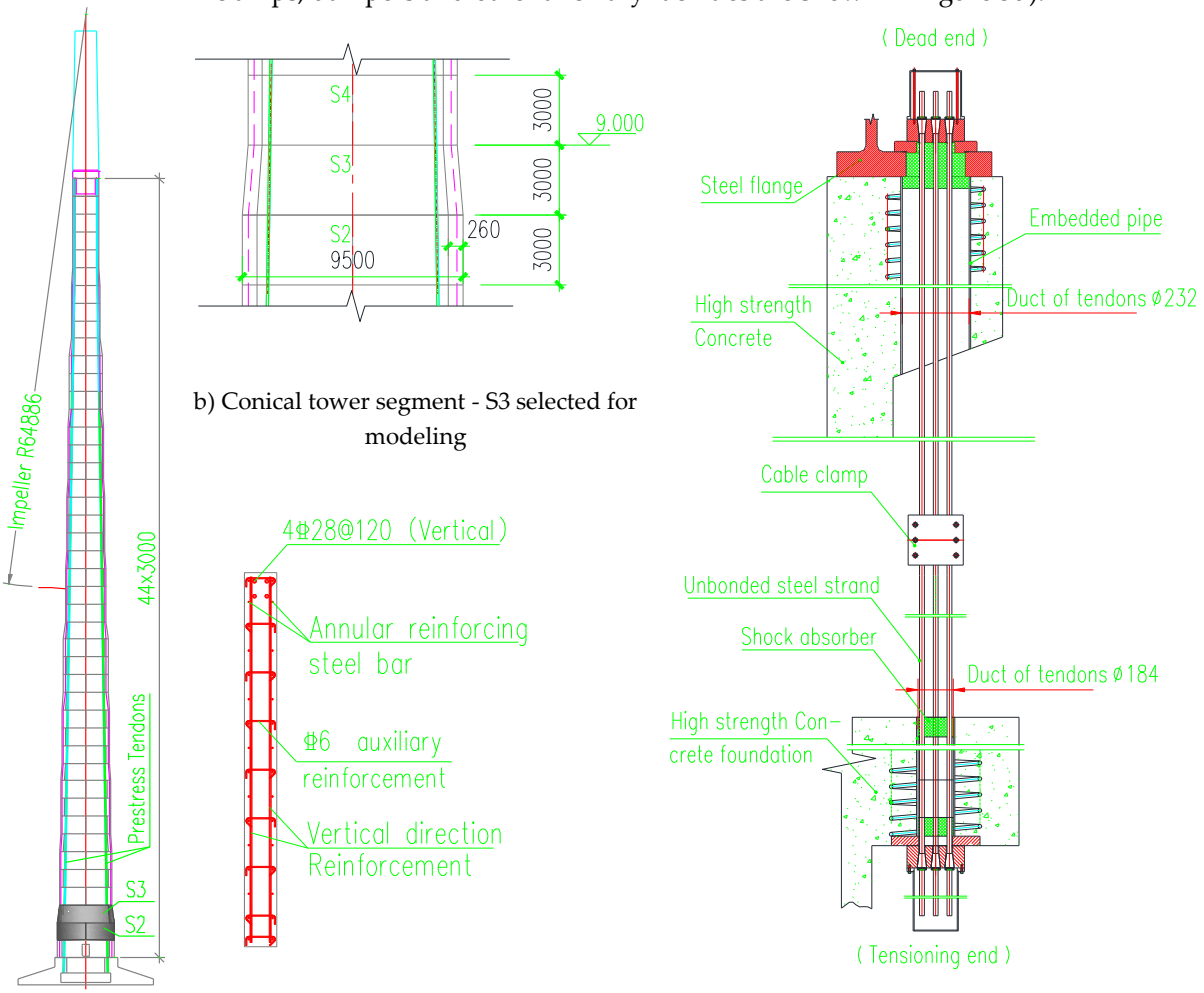

a) Elevation view

b) Conical tower segment - S3 selected for modeling

c) Reinforcement diagram of segment S3 of the tower

d) Schematic of the longitudinal prestressing system

Figure 3 Structural diagram of the precast concrete tower

In this design, a basic unit is consisted by several straight cylinder segments connected with a conical segment to reduce the diameter to the next level, to make the tower outer diameter gradually reducing from 9.5m at the base to 4.5m at the top of the concrete portion. Three circumferential prestressed steel strands are designed at the lower 1/3 of the height of each conical segment to apply circumferential prestressing.

In the following calculations, the conical tower segment closest to the foundation (the 3rd segment from the bottom, hereinafter referred to as segment S3, as shown in Figure 3b)) is selected for modeling and analysis. The wall thickness of segment S3 of the tower is 260 mm, the top diameter is 9,000 mm, the bottom diameter is 9,500 mm, and the height is 3,000 mm. The concrete grade applied to the full tower is C75 (cube strength), and the reinforcement layout of the tower segment is shown in Figure 3c). In the circumferential direction, there are a total of 32 Φ12 (32 reinforcement bars with a strength grade of HRB400 and a diameter of 12 mm.) Circumferential reinforcement bars were evenly distributed along the height of the tower in the two layers inside and outside. At 100 mm, 350 mm, and 600 mm from the bottom end, a low-relaxation prestressed steel strand ϕ^s15.2 is placed at each

 https://doi.org/10.59238/j.pt.2024.03.003

height, with a tensile strength f_{ptk} of 1,860 MPa. When each strand is tensioned, the applied prestress is $0.7f_{ptk}$. After various prestressing losses are considered, the final effective tension design value is $0.45f_{ptk}$, which is 117.18 kN. Straight cylinder segment S2 (beneath segment S3) has the same top diameter as the bottom diameter of segment S3, which is 9,500 mm, the bottom diameter of S2 is 9,500 mm, the height is 3,000 mm, and the thickness is 260 mm. The circumferential reinforcement setting is the same as that of segment S3. In addition, four circumferential reinforcement bars ⌀28 are additionally arranged at the top of segment S2 to increase the circumferential stiffness at the top of segment S2.

In a certain wind power project, the above-mentioned scheme design is adopted, and one of the three circumferential steel strands in segment S3 is combined with an optical fiber to create a CFRP-OFBG intelligent steel strand for prestress monitoring. During the processing and production of the FRP bars, the optical fiber grating is sent into the mold cavity in parallel. After passing through the high-temperature and high-pressure mold cavity, the optical fiber grating is coupled in the center of the FRP, as shown in Figure 4. The grating sensor and the FRP carry out strain measurements based on the principle of synergistic deformation. In this way, the produced FRP material is embedded with a fiber grating sensor with sensing characteristics, and the tensile strength of the CFRP bar is greater than 2,000 MPa.

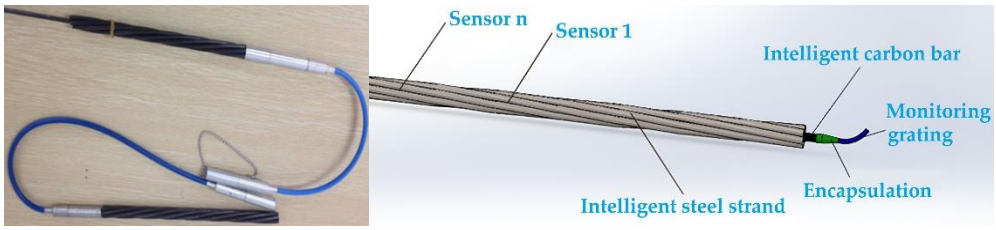

Figure 4 Schematic of the intelligent steel strand

In the actual measurement, four measuring points are taken for the recording of the circumferential intelligent steel strand (Figure 5). Before the tensioning of the smart steel strands, the initial wavelength λ_0 was measured through the embedded grating sensor. During the circumferential prestressing tensioning, the wavelength data measured by the embedded grating sensor were used. By calculating the change in wavelength before and after, the strain value of the steel strand can be derived, which then allows for the calculation of the actual prestress force F of each intelligent steel strand. Detailed monitoring data are shown in Table 1. It can be seen, the prestress loss is greater at measurement points 1 and 4, which are close to the tensioning ends, leading to slightly lower stress values. In contrast, the prestress loss is smaller at measurement points 2 and 3, resulting in higher stress values. Considering that the circumferential steel strands are tensioned from both ends and that there is some overlap where the strands loop around, the relatively low prestress measurement values at points 1 and 4 do not affect the prestress applied to the main body of the structure.

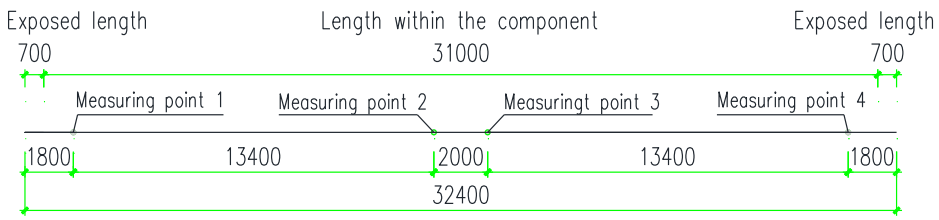

Figure 5 Measuring points of the circumferential intelligent steel strand in segment S3

Note: The length of reading leading wire of S3 intelligent steel strand is 8 m.

Table 1 Monitoring data of the circumferential intelligent steel strand in segment S3

Measuring Point	Initial Wavelength λ_0 (nm)	Measured Wavelength λ_i (nm)	Measured Force F (kN)	Theoretical Calculated Force F_0 (kN)	Percentage F/F_0
Point 1	1,536.006	1,542.209	163.8	165.9	98.78%
Point 2	1,540.567	1,546.299	151.4	131.5	115.11%
Point 3	1,545.213	1,551.519	166.6	125.5	132.69%
Point 4	1,550.089	1,553.721	95.9	108.3	88.55%

3 Simplified Calculation of the Structural Forces in the Conical Segment

The structural parts near the nonvertical joints can be approximately regarded as the whole-ring segment structure for simplified analysis (Figure 6), whereas near the vertical joints, it is difficult to obtain the role of circumferential prestressing in the structural force balance through simplified calculations because of the more complex force situation. Under the action of service loads, the annular horizontal joints are fully compressed under the whole section, and the strut-and-tie model can be used to simplify the analysis of the stress state of the reinforcement at the top of segment S2 and the bottom of segment S3 (not suitable for cases where one side of the horizontal joint of the tower partially separates under ultimate loads). The external load acting on the top of the conical segment is applied to the center of the top surface, a narrow unit with a width of $d\theta$ in the circumferential direction is taken for the force analysis of the strut-and-tie model, and the equivalent compressive stress of the external load is applied to the centroid of the corresponding arc.

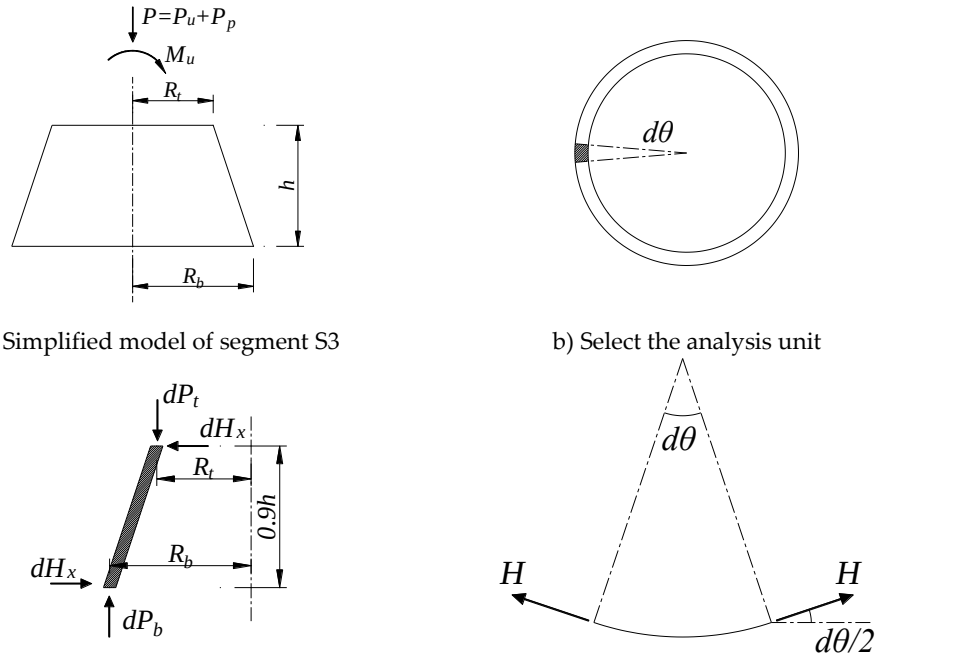

a) Simplified model of segment S3 b) Select the analysis unit

c) Strut-and-tie model of the analysis unit d) Circumferential tension of the analysis unit

Figure 6 Simplified calculation model of the structural forces of the conical segment S3

The vertical force dP_t applied to the top of the analyzed unit within the $d\theta$ width range is shown in Equation (1), and the vertical force dP_b applied to the bottom of the analyzed unit is shown in Equation (2). Disregarding the self-weight of this segment of the tube wall (the top external load and the tension of the steel strand on the tube are much greater than the self-weight of this segment of the tower structure), let $dP_t = dP_b$, where the maximum values of the compressive stresses σ_{vt} and σ_{vb} on the upper section and lower section, respectively, of the tube wall are shown in Equations (3) and (4), respectively. Taking the moment dM at the top of the

 https://doi.org/10.59238/j.pt.2024.03.003

segment, the moment generated by the vertical force is shown in Equation (5), the moment dM generated by the horizontal force is shown in Equation (6), and the radial component dH_x of the tension of the circumferential reinforcement and the steel strand is shown in Equation (7).

$$dP_t = \sigma_{vt} \cdot R_t \cdot d\theta \cdot t_t \tag{1}$$

$$dP_b = \sigma_{vb} \cdot R_b \cdot d\theta \cdot t_b \tag{2}$$

$$\sigma_{vt} = \frac{P}{A_t} \pm \frac{M}{W_t} \tag{3}$$

$$\sigma_{vb} = \frac{P}{A_b} \pm \frac{M}{W_b} \tag{4}$$

$$dM = dP_b(R_b - R_t) \tag{5}$$

$$dM = dH_x \cdot 0.9h \tag{6}$$

$$dH_x = 2H\frac{d\theta}{2} \tag{7}$$

where R_t and R_b are the radius at the top and bottom sections of the conical segment S3; t_t and t_b are the wall thicknesses at the top and bottom; h is the height of the conical segment; W_t and W_b are the sectional modulus of the top and bottom surfaces of this segment, respectively.

Under the plane-section assumption, the upper half of conical segment S3 is circumferentially compressed, and the lower half of the conical segment S3 is circumferentially tensioned. The top of the straight cylinder segment S2 is circumferentially tensioned, and the bottom is circumferentially subjected to very little force. Conservatively, if the tensile stress in the concrete is disregarded, the circumferential tension is assumed to be carried by the circumferential reinforcing bars and the circumferential prestressed steel strands within the lower 1/3d of conical section S3, and the circumferential reinforcing bars within the upper 1/3d of cylindrical section S2. The service applied service load M and P on the top position of the segment S3 are 124,647 kN·m and 62,926 kN respectively. After sorting, the circumferential tension is shown in Equation (8). The total tension of the three steel strands with an effective stress of $0.45f_{ptk}$ is 480 kN, and the remaining tension is borne by the reinforcement. The tensile stress of the reinforcement is 153.6 MPa, which is less than the yield stress of the reinforcement, as shown in Equation (9).

$$H = \left(\frac{P}{2\pi} + \frac{M}{\pi R_b}\right) \cdot \frac{R_b - R_t}{0.9h} = \left(\frac{62926}{2\pi} + \frac{124647}{\pi \times 9.5}\right) \times \frac{4.62 - 4.37}{0.9 \times 3} = 1314\ \text{kN} \tag{8}$$

$$\sigma_{st} = \frac{H - T_p}{A_s} = \frac{1314 - 480}{5428} \times 10^3 = 153.6\text{Mpa} \tag{9}$$

4 Finite Element Model

The finite element software Abaqus is used to establish and solve the model in the research and analysis. The coordinate system of the model is shown in Figure 7, where the origin of the coordinate system is located at the center of the bottom surface of tower S2, gravity is along the negative direction of the y-axis, and a vertical splicing joint of tower S3 is located above the positive direction of the x-axis. The tower structure is simulated by a three-dimensional, eight-node reduced integration solid element, C3D8R, and the reinforcement and circumferential prestressed steel

strands are simulated by a three-dimensional, two-node truss element, T3D2, embedded in the concrete tower segment [4]. The circumferential prestress at the bottom of the conical segment is simulated by applying a temperature field load (cooling) to the prestressed steel strands, whereas longitudinal prestressing is introduced into the model by applying a vertical external load. The circumferential and vertical splicing joints between the tower segments are set to allow for tangential finite sliding contact, and the friction coefficient is 0.5. At the center of the top surface of tower segment S3, the action point of the external load concentrated force is defined. To prevent stress concentration caused by the application of a concentrated force, this action point is coupled with the top surface element of segment S3. Owing to the regular geometric shape of the structure, the structural mesh adopts a hexahedral mesh. For each tower segment, the circumferential direction is divided into 120 equal parts, the radial direction is divided into 4 equal parts, and the longitudinal direction is divided into 20 equal parts.

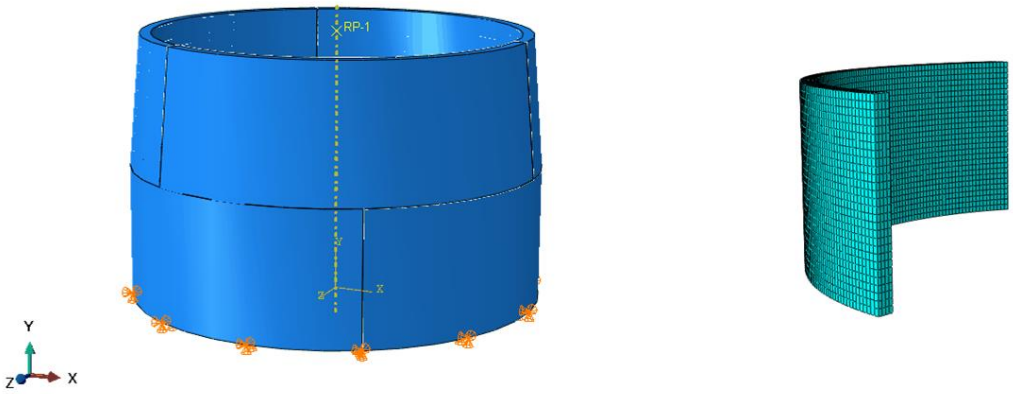

Figure 7 Finite element model, coordinate system, boundary conditions, and mesh division of tower segments

To simulate the real service state of the tower, the load is applied in three steps: (1) Initial condition: Gravity, circumferential prestressing load, and longitudinal prestressing load are applied. (2) Service condition: The service loads are applied. (3) Ultimate condition: The ultimate loads are applied.

The magnitude of the circumferential prestressing load is defined by the tensioning scheme, as described in the following schemes. The other ultimate loads applied to the top of segment S3 are calculated and given by the wind turbine main engine manufacturer, as shown in Table 2 and Figure 5. In the calculation, 60% of the ultimate loads are taken as the normal service loads and are listed in Table 2.

Table 2 Service and ultimate design load combinations at the top of segment S3 of the tower

Items	Service Loads	Ultimate Loads
Transverse Force F_z (kN)	926.4	1,534
Longitudinal Force F_y (kN)	62,926	64,633
Bending Moment M_x (kN·m)	124,647	221,581
Torsion M_y (kN·m)	1,558.8	2,598

Since, in the working state defined in this example, the elastoplastic state of the concrete may have exceeded the elastic state and entered the plastic state, its elastoplastic properties need to be considered when defining the concrete material. Here, the concrete plastic damage model [5,6] is selected to describe the constitutive relationship of concrete. The stress–strain curves of the concrete are shown in Figure 8.

 https://doi.org/10.59238/j.pt.2024.03.003

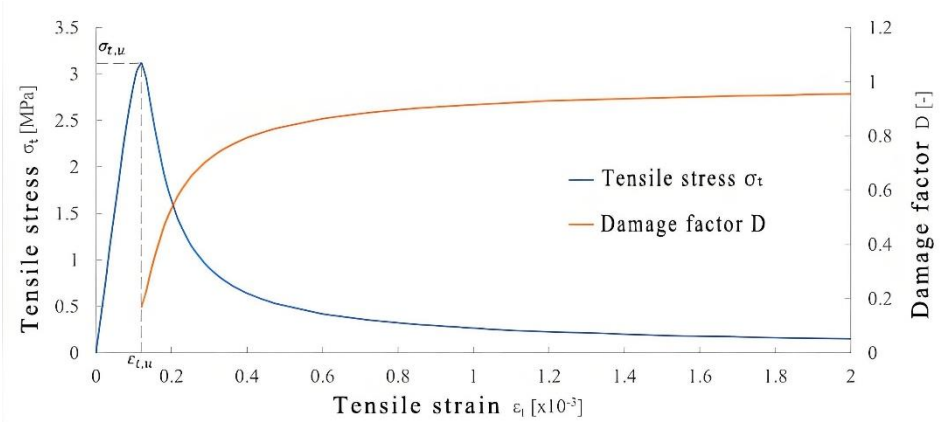

a) Tensile stress–strain curve

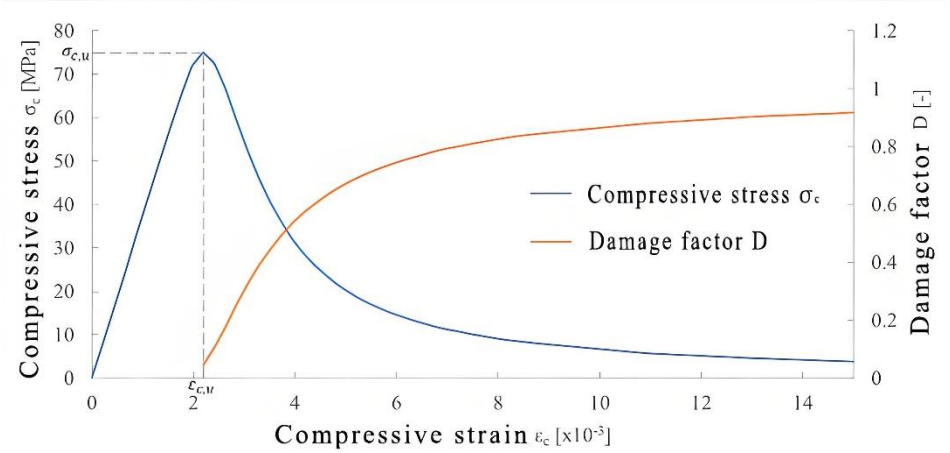

b) Compressive stress–strain curve

Figure 8 Concrete stress–strain curves used in the finite element model

To compare the constraining effects of circumferential prestressing and ordinary reinforcement bars on the precast tower structure, the model compares and analyzes the following situations. The reinforcement design in Scheme A is as described in Chapter 2. In Scheme B, 8 ⌀16 circumferential steel bars in 4 groups at the bottom of conical segment S3 are used, the remaining 24 ⌀12 steel bars in 12 groups continue to be used, and the other parameters are the same as those in Scheme A. Compared with Scheme B, in Scheme C, the circumferential steel strand of conical segment S3 uses ϕ^s17.8, and the prestressing tensioning scheme is designed so that the effective prestressing force after the prestressing loss being applied is the same as that in Scheme B. In Scheme D, the other parameters are the same as those in Scheme B, and the difference is that the control tension force during construction is increased so that the effective stress after the prestressing loss being applied is $0.5f_{ptk}$. A comparison of the four schemes is shown in Table 3. To simplify the model, the influence of vertical reinforcement is not considered in the simulation.

Table 3 Comparison of different FEM simulation schemes

Scheme Number	Circumferential reinforcement of the conical segment	Circumferential stiffeners at the top of the straight segment	Circumferential prestressed steel strand	Circumferential prestress
A	32⌀12	4⌀28	$3\phi^s$15.2	$0.45f_{ptk}$
B	24⌀12 + 8⌀16	4⌀28	$3\phi^s$15.2	$0.45f_{ptk}$
C	24⌀12 + 8⌀16	4⌀28	$3\phi^s$17.8	$0.45f_{ptk}$
D	24⌀12 + 8⌀16	4⌀28	$3\phi^s$15.2	$0.50f_{ptk}$

The simulation scheme is designed in this way to achieve the following research purposes:

(1) By comparing schemes A and B, the effect of increasing the reinforcement ratio to enhance the stiffness of the bottom of the conical section is explored.

(2) By comparing schemes B and C, the effect of increasing the prestress level through increasing the cross-sectional area of the prestressed steel strands is explored.

(3) By comparing schemes B and D, the effect of increasing the prestress level by increasing the tensioning force while keeping the cross-sectional area of the prestressed steel strands unchanged is explored.

5 Model Results Analysis

5.1 Structural Response of Scheme A under the Service Load

For Scheme A, under the action of the service load, the deformation of tower segments S2 and S3 is shown in Figure 9. The maximum displacement of the tower segment occurs in the horizontal direction along the direction of the transverse external force. The maximum opening of segment S2 at vertical joint A is 0.92 mm. Moreover, owing to the influence of the bending moment and torsion, vertical joint D opens horizontally by 0.64 mm, which is significantly greater than that of vertical joint F (0.14 mm). In addition, a horizontal opening of 0.17 mm is also observed at vertical joint C. The openings at other locations are not significant (less than 0.1 mm).

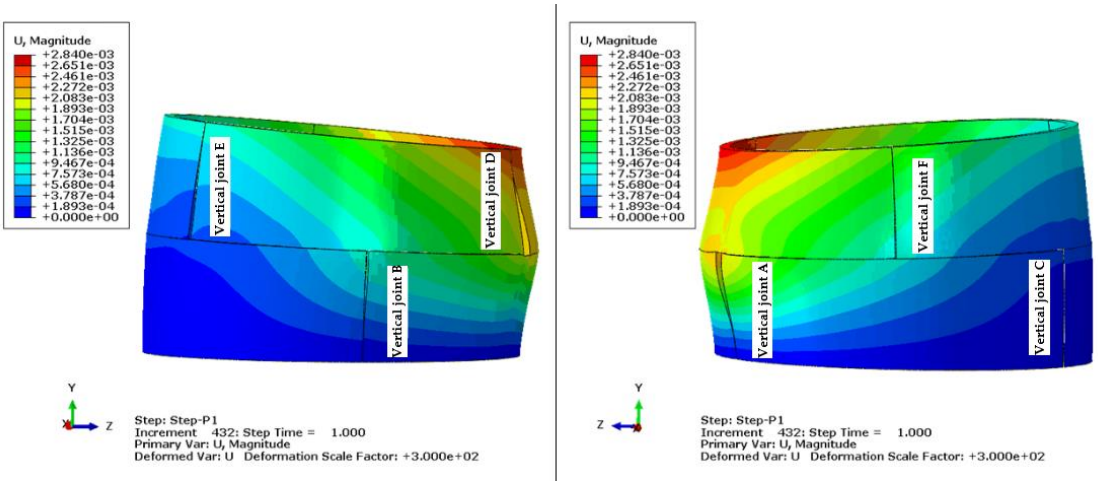

Figure 9 Structural deformation of scheme a under the service load

Figure 10 shows the distribution of the compressive stress (Figure 10 a)) and the theoretical calculated value (Figure 10 b)) on the horizontal joint between S2 and S3. Under the service load, the maximum compressive stress on the compression side is 15.6 MPa (disregarding the stress at the edge of the local vertical joint in the finite element model), and the finite element simulation value is consistent with the theoretical value. The maximum compressive stress occurs below vertical joint D, which is also the location with the largest deformation.

Figure 11 shows the maximum principal stress (that is, the main tensile stress of the concrete) of the concrete in tower segments S2 and S3 under the service load. The maximum principal stress of conical segment S3 corresponds directly above the opening of vertical joint A, whereas the maximum principal stress of straight cylinder segment S2 is located below the opening of vertical joint D, with stress values of 2.995 MPa and 2.825 MPa, respectively. The damage factor of concrete shown in Figure 12, some of the concrete has entered the plastic state, and two vertical cracks start to spread vertically from these two points to the other end of the tower.

 https://doi.org/10.59238/j.pt.2024.03.003

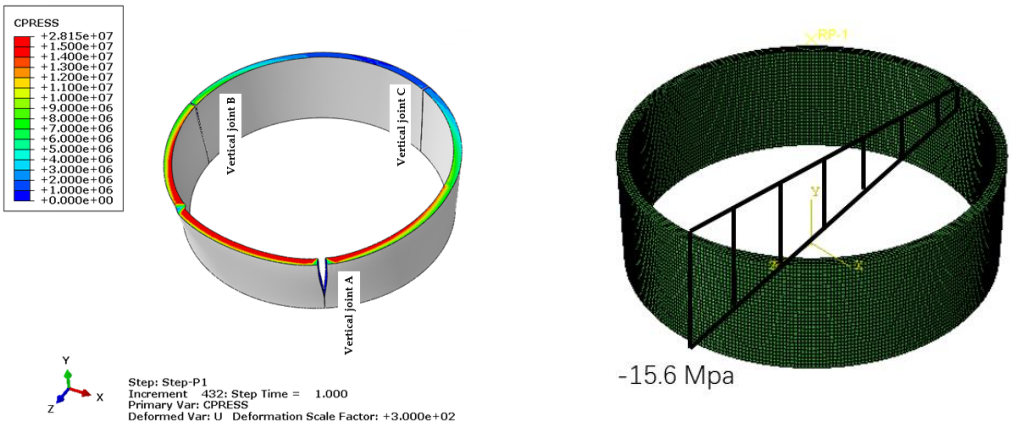

a) Simulation value b) Theoretical calculated value

Figure 10 Stress distribution at the horizontal joint between S2 and S3

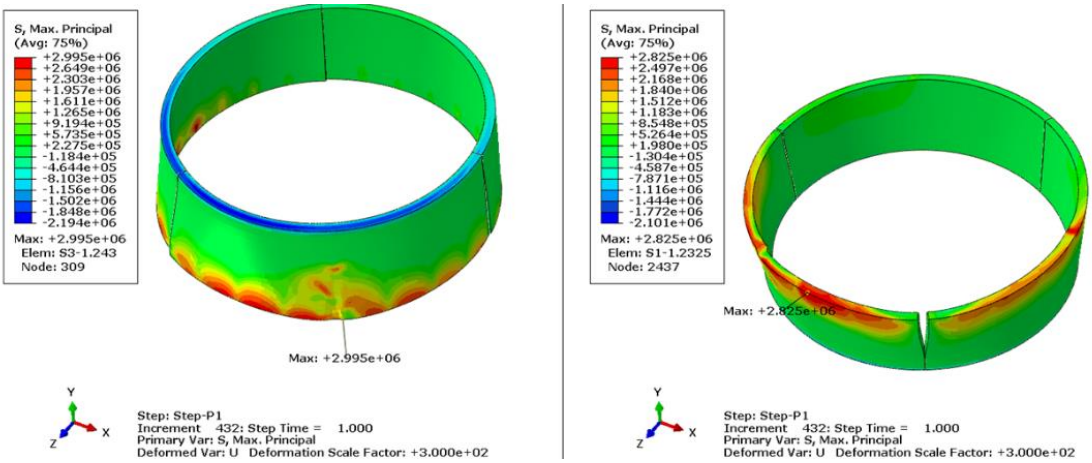

Figure 11 Maximum principal stress of the concrete in tower segments S2 and S3

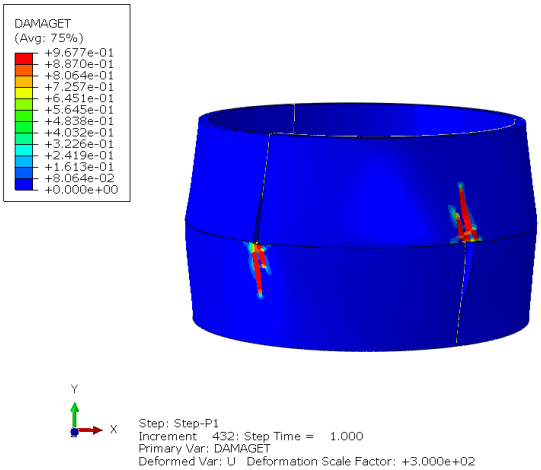

Figure 12 Concrete damage factor of the structure under the service load

Figures 13 and 14 show the stress states of the reinforcement and steel strands, respectively, in the tower segment under the service load. The maximum stress positions of the tower segment reinforcement are easily observed to be the same as the maximum positions of the concrete. The maximum tensile stresses of the horizontal reinforcement in segments S2 and S3 are 54.1 MPa and 120.7 MPa, respectively. The maximum tensile stress of the steel strand configured in conical segment S3 appears at vertical joint A, which is 944.3 MPa, an increase of 12.8% compared with the initial prestress of 837 MPa.

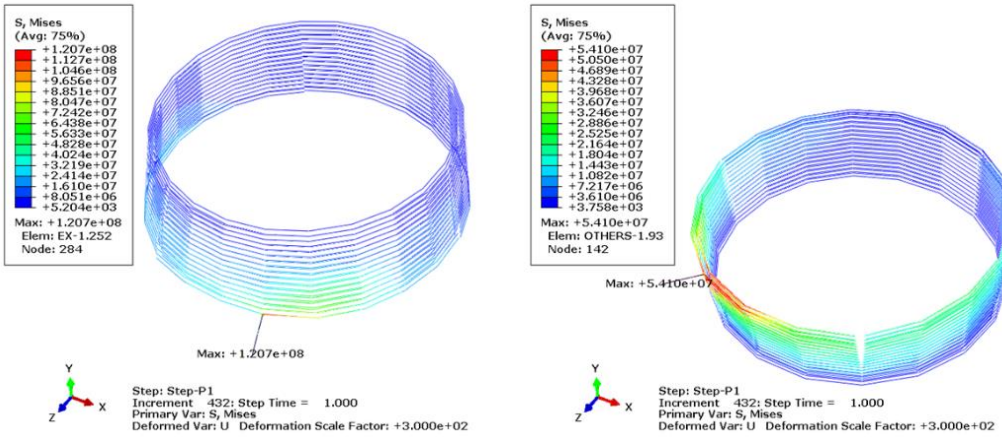

a) Segment S3 b) Segment S2

Figure 13 Tensile stress of the circumferential reinforcement of the tower

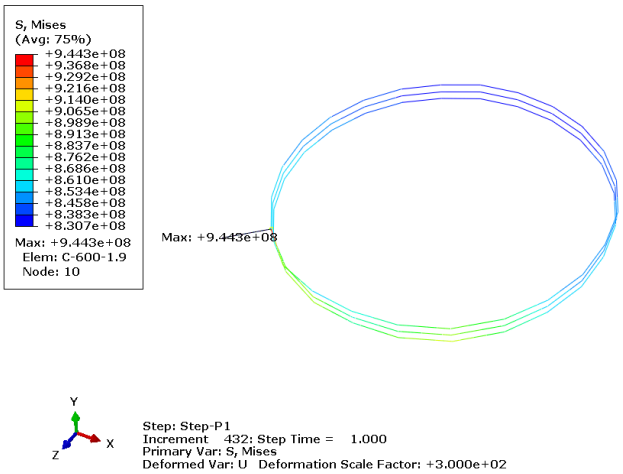

Figure 14 Tensile stress of the prestressed steel strand

A comparison of the circumferential reinforcement stresses of tower segments S2 and S3 in Figure 13 reveals that the circumferential reinforcement stress at the top of segment S3 is approximately 2.2 times greater than the circumferential reinforcement stress at the bottom of segment S2. In the comparison of Schemes B, C, and D, the stress state of this part is optimized by increasing the circumferential reinforcement at the bottom of segment S3, increasing the cross-sectional area of the prestressed steel strand at the bottom of segment S3, and increasing the circumferential steel strand prestress of segment S3. These measures are aimed at reducing the stress value in the circumferential reinforcement and decreasing the tensile stress in the concrete circumferential direction. Essentially, this brings the stress level of the circumferential reinforcement in the lower part of conical segment S3 closer to that of the circumferential reinforcement at the top of adjacent cylindrical segment S2. In other words, it ensures that the stiffness in the circumferential direction of these two segments is similar.

5.2 The Optimization Effect of Scheme B of Increasing Reinforcement on Structural Response

A comparison of Schemes A and B, with the circumferential prestressing remaining unchanged, reveals that only the 4 groups of 8 steel bars at the bottom increase from ⌀12 to ⌀16. Table 4 lists the impact of this change. The increase in the cross-sectional area of the reinforcement in segment S3 enhances its stiffness, thereby reducing the opening of the vertical joints in both straight cylinder segment S2 and conical segment S3, with the maximum values reduced by 10% and 1.6%, respectively.

 https://doi.org/10.59238/j.pt.2024.03.003

Owing to the increase in the circumferential stiffness, the tensile stress of the reinforcement in conical segment S3 also decreases.

Table 4 Structural responses before and after increasing the reinforcement at the bottom of the conical segment

Scheme Number	Scheme A	Scheme B	Rate of change
Segment S2 maximum vertical joint opening value (mm)	0.92	0.827	-10.1%
Segment S2 maximum concrete tensile stress (MPa)	2.83	2.81	-0.5%
Segment S2 maximum reinforcement tensile stress (MPa)	54.10	53.94	-0.3%
Segment S3 maximum vertical joint opening value (mm)	0.64	0.63	-1.6%
Segment S3 maximum concrete tensile stress (MPa)	2.995	3.053	1.9%
Segment S3 maximum reinforcement tensile stress (MPa)	120.70	108.1	-10.4%
Segment S3 maximum prestressed steel strand tensile stress (MPa)	944.30	944.2	0.0%

5.3 The Optimization Effect of Scheme C and Scheme D of Increasing Prestressed Load on Structural Response

Comparing Scheme B and Scheme C, the steel strand specification increases from ϕ^s15.2 to ϕ^s17.8, with the corresponding cross-sectional area increases from 140 mm² to 191 mm². Since the prestressing value remains unchanged, it is equivalent to an increase in the effective tension force of 37.9%.

Comparing Scheme B and Scheme D, with the other conditions remaining unchanged, the prestressing is increased from 837 MPa in the initial design to 930 MPa, which is equivalent to an increase in the effective tension force of 11.1%. Both schemes increase the tension force, and the increase ratio of Scheme C is greater. Table 5 lists the impacts of the changes in the two schemes.

Table 5 Structural responses before and after increasing the prestressing tension at the bottom of the conical segment

Scheme Number	Scheme B	Scheme C	Rate of change	Scheme D	Rate of change
Segment S2 maximum vertical joint opening value (mm)	0.827	0.714	-13.6%	0.792	-4.22%
Segment S2 maximum concrete tensile stress (MPa)	2.81	3.26	15.9%	2.85	1.42%
Segment S2 maximum reinforcement tensile stress (MPa)	53.94	45.08	-16.4%	48.91	-9.33%
Segment S3 maximum vertical joint opening value (mm)	0.63	0.45	-28.3%	0.52	-1.59%
Segment S3 maximum concrete tensile stress (MPa)	3.053	2.95	-3.3%	2.951	-3.34%
Segment S3 maximum reinforcement tensile stress (MPa)	108.1	67.63	-37.4%	74.26	-31.30%
Segment S3 maximum prestressed steel strand tensile stress (MPa)	944.2	896.60	-5.0%	998.2	5.72%

The impacts of the two schemes are basically the same; that is, they reduce the tensile stress of the reinforcement and the opening value of the vertical joint in segments S2 and S3. Owing to the large increase, the effect of Scheme C is more significant. However, these two schemes also lead to an increase in the tensile stress of the concrete in segment S2.

5.4 Structural Response of the Optimal Scheme C under Ultimate Load

Table 6 shows the responses of segments S2 and S3 of the tower designed according to Scheme C under the ultimate load. Owing to the limitation of computing resources, the vertical joints are not considered in the finite element calculation and analysis under the ultimate load; that is, it is assumed that segments S2 and S3 are both full-ring structures. Overall, the horizontal joint between the two segments will open under the ultimate load, with a maximum value of 4.49 mm (Figure 15). Compared with the operational load conditions of this scheme, the stresses, and deformations of all the components of the tower wall are significantly greater under the service load conditions. However, since the important structural features of the vertical joint model are disregarded in this calculation, the results may be biased and should be further explored.

Table 6 Structural response of Scheme C under the ultimate load

Scheme Number	Scheme C
Segments S2 and S3 maximum horizontal joint opening value (mm)	4.49
Segment S2 maximum concrete tensile stress (MPa)	3.86
Segment S2 maximum reinforcement tensile stress (MPa)	126.2
Segment S3 maximum concrete tensile stress (MPa)	3.076
Segment S3 maximum reinforcement tensile stress (MPa)	155.5
Segment S3 maximum prestressed steel strand tensile stress (MPa)	983.2

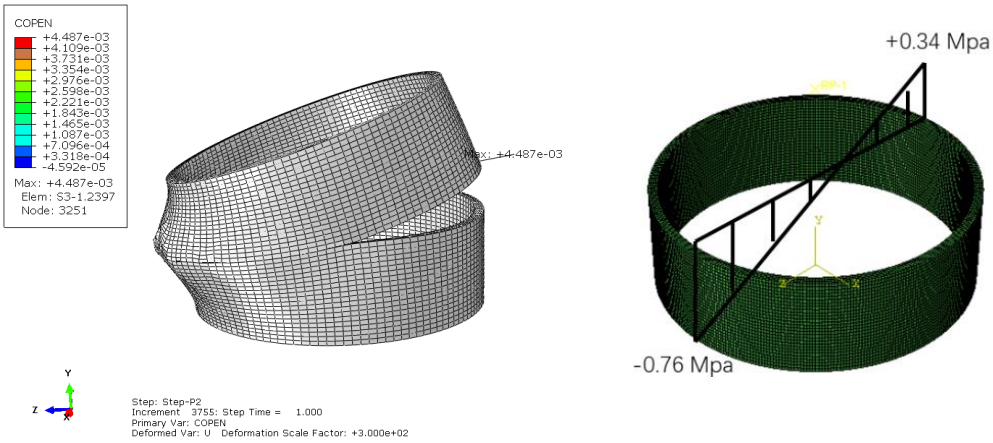

a) Simulation value b) Theoretical calculated value

Figure 15 Deformation of the segments S2 and S3 under the ultimate load conditions

6 Conclusion

In this paper, the application of circumferential prestressing technology in precast concrete wind turbine tower structures are studied through simplified calculations and finite element simulations. The research results show that appropriately adjusting the circumferential reinforcement ratio or the level of prestressing tension force at the bottom of the tower conical segment with circumferential prestressing can significantly optimize the performance of the structure under the applied turbine loads. In actual design, the above adjustment is equivalent to changing the circumferential structural stiffness of the adjacent tower segments, which can achieve the optimal configuration of the structure.

https://doi.org/10.59238/j.pt.2024.03.003

Conflict of Interest: All authors disclosed no relevant relationships.

Data Availability Statement: The data that support the findings of this study are available from the corresponding author, Wei, upon reasonable request.

References

1. Liu, R.; Sun, X.; Ye, H. Study on Mechanical Performance of Large Diameter Composite Supporting Tower for Wind Turbines. *Structural Engineers* **2023**, *39*, 39-45, doi:10.3969/j.issn.1005-0159.2023.01.006.
2. Zhang, H.; Wei, B. Construction Technology and Application of Bonded Pre-stressed Tendons in Wind Turbine Mixed Towers. *Prestress Technology* **2024**, *2*, 70-80, doi:10.59238/j.pt.2024.02.006.
3. China Concrete and Cement Products Association. Research and Application of the Key Technology of 160 m Grade Precast Concrete-steel Hybrid Tower. Available online: https://www.ccpa.com.cn/site/content/12084.html (accessed on 2024-02-14).
4. Qiang, X.; Hu , W.; Hu, G.; Jiang, X.; Tang, Y. Theoretical and Numerical Analysis of Reinforced Concrete Beams Strengthened with Externally Prestressed CFRP Bars. *Structural Engineers* **2024**, *40*, 465-174, doi:10.3969/j.issn.1005-0159.2024.01.020.
5. Ministry of Housing and Urban-Rural Development of the People's Republic of China. GB 50010—2010 Code for Design of Concrete Structures. China Architecture Publishing & Media Co., Ltd.: Beijing, 2011.
6. Liu, W.; Xu, M.; Chen, Z. Parameters Calibration and Verification of Concrete Damage Plasticity Model of Abaqus. *Industrial Construction* **2014**, *44*, 167-171,213, doi:10.13204/j.gyjz2014.s1.227.

AUTHOR BIOGRAPHIES

Kangle Chen
Dr.–Ing., Shanghai Zhengruida Renewable Energy Co., Ltd.
Research Direction: Structural Design and Optimization of Wind Turbine Tower.
Email: chenkangle@zwindtowers.com

Di Yao
M.Sc., Shanghai Zhengruida Renewable Energy Co., Ltd.
Research Direction: Structural Design and Optimization of Wind Turbine Tower.
Email: yaodi@zwindtowers.com

Sihang Wei
PhD, Shanghai Zhengruida Renewable Energy Co., Ltd.
Research Direction: Structural Design and Optimization of Wind Turbine Tower.
Email: weisihang@zwindtowers.com